A 'molecular' description of current flow

Avik W. Ghosh, Kamaram Munira and Mikiyas Tsegaye

School of Electrical and Computer Engineering, University of Virginia, Charlottesville 22904, USA

Abstract— We present a unified formalism for describing current flow through any small 'molecule'. The formalism can be translated into 'first principles' simulations towards predictive properties with no adjustable parameters. Three case studies are presented – electron spectroscopy in buckyballs on silicon, spin currents and torques in an Fe-MgO-Fe tunnel junction, and thermal currents in graphene nanoribbons. In each case, a 'molecular' description is critical to the underlying physics.

Modern day electronics is rapidly reaching nanometer dimensions where atomistic, quantum and many-body effects dominate. The non-equilibrium Green's function (NEGF) approach provides a systematic way to handle these effects. The channel bands are described by a Hamiltonian H and potential U, while the contact thermal reservoirs are described by self-energy matrices $\Sigma_{1,2}$ (Fig. 1). Dephasing is described by additional self-energies Σ_s. By solving the resulting Schrodinger equation with open non-equilibrium boundary conditions set by the contact Fermi functions (with unequal electrochemical potentials $\mu_{1,2}$), we can arrive at a rigorous theory for current flow through any nano-device. The predictive power thereafter depends on the degree of sophistication of the input matrices.

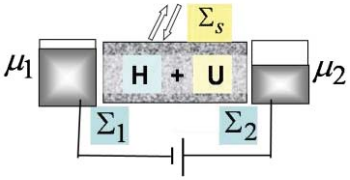

Fig.1. A schematic description of current flow in NEGF

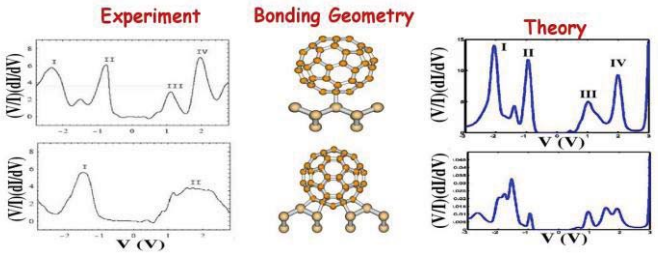

Fig. 2. NEGF-DFT treatment of C60 spectra on Si reproduces experimental variations attributed to alterations in bonding geometry at the interface (adapted from [1]).

Fig. 2 shows the computed current through fullerene adsorbed on a silicon surface. Similar theories can be invoked to describe current flow through other molecules, nanowires, nanotubes, graphene, and quantum dots. The challenge is to engineer the bonds for optimal barrier heights for injection, and maximal charge conjugation for adequate current.

Fig. 3 shows the computed characteristics in an Fe-MgO-Fe spin transfer torque random access memory (STTRAM). We can use our NEGF equations to compute the device characteristics. The injected electrons are polarized by the first (fixed) Fe layer and tunnel across the MgO to the second (free) Fe layer. The spin angular momentum components perpendicular to the free layer get completely absorbed, making the latter magnetization precess until the torque is sufficient to overcome the restorative damping forces and go beyond the equatorial plane (right). A 'molecular' understanding of spintronics is critical to the suitable design of an STTRAM. An atomistic theory shows that the critical switching current can be lowered by selectively filtering the Fe majority spins by the complex Δ_1 tunneling bands in MgO.

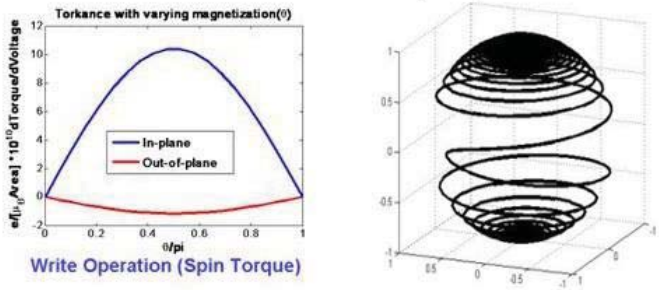

Fig.3. (Left) Computed spin torques, and (right) precession dynamics of free layer in an Fe-MgO-Fe sandwich.

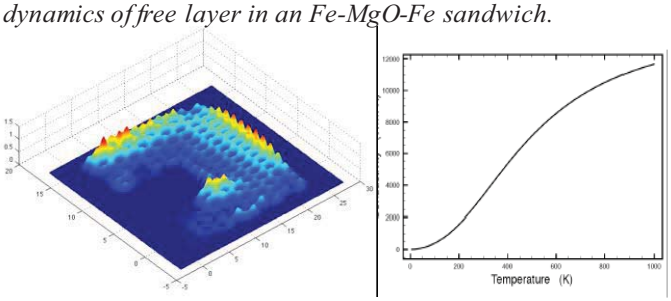

Fig.4. (Left) Computed thermal 'hot spots' in a graphene U-junction, and (right) the bulk graphene thermal conductivity.

The final example comes from thermal flow. Fig. 4 (left) shows the computed thermal current in a graphene U-junction, showing the location of thermal 'hot spots'. This requires a molecular description of defect states (such as edges and bends). Furthermore, the computed bulk conductivity in a graphene sheet is also shown (right). The room temperature values agree favorably with experiments in the literature. The NEGF formalism allows us to interpolate between Fourier's law (Fig. 4), and the ballistic limit where the entire thermal conductance is quantized. Once again, a molecular level model incorporating the proper graphene chemistry helps understand the underlying processes in complicated nanoribbons fabricated out of the graphene templates.

In summary, by combining a molecular description of bonding and charge delocalization with the non-equilibrium quantum flow of electrons, we can compute the flow of 'anything through anything', that is critical to the development of novel applications for logic, memory and communication beyond the limits of today's silicon-based CMOS technology.

*Corresponding author: ag7rq@virginia.edu

[1] G-C. Liang and A. W. Ghosh, Phys. Rev. Lett. 95, 076403 (2005).

Assembly of Nanostructures: From Self-Assembly to Directed Assembly

Mustafa Çulha*

Yeditepe University, Faculty of Engineering and Architecture, Department of Genetics and Bioengineering, 34755 Kayisdagi-Istanbul, Turkey

Abstract— The assembly of nanostructures into higher organizations remains to be one of the major challenges in applications of nanotechnology, which has critical importance for construction of novel surfaces and interfaces with unique physicochemical properties. In order to manage to direct the nanostructures into desired locations and orientations, it is necessary to fully understand the forces governing their behavior under the studied system. In this study, a summary of our effort to utilize the droplets as tools to manipulate the nanostructures on surfaces is presented.

With their fascinating physicochemical properties, nanostructured materials are holding enormous prospects in many fields of science and technology. However, the two major bottlenecks in applications of nanostructured materials, their uniform synthesis and assembly into targeted structures at surfaces and interfaces, still remain the major challenge [1]. Although there are some advances have already made to overcome some of the difficulties, it seems that the challenges will remain until a comprehensive understanding of the forces influencing the behavior of nanostructures or being able to control them by learning the use of already know forces.

There are currently a number of ways that can be pursued for the directing the nanostructures into the desired patterns. All lithographic techniques uses a template generated either using a mould, light or electron beam [2]. Although a certain level of success can be easily achieved using the lithographic techniques, they are rather crude and are currently far from the precise alignments of the nanostructures.

Another approach is to use the molecular forces to bring the nanostructures into desired orientations. In this group of approaches, a molecule that is well known for its molecular behavior is chemically attached the nanostructure. Due to the excreted molecular force on the nanostructure, it is forced to balance the excreted force by locating itself into the patterned structure. This approach can be considered as a utility of the molecular assembly for the assembly of the nanostructures. In our studies, we utilize biomacromolecular structures not only to understand the molecular forces influencing the behavior of nanotructures at interfaces but also use the well defined forces such as DNA hybridization to construct higher structures using nanostrucures as building blocks [3].

In this presentation, our findings on the control of the nanoparticles from a drying droplet and the influence of the surface properties of nanoparticles which was systematically altered with peptides, carbohydrates, lipids at liquid-solid interface are presented along with the directed assembly of AuNPs using DNA hybridization. The manipulation of nanoparticles residing in a suspension by physical means is also perused. Figure 1 shows the reversal of the assembly of latex particles using a hydrophobic tip, which was located on the top of the drying droplet. For example, touching or dipping a hydrophilic or hydrophobic tip on/into a drying droplet can alter the packing or assembly of nanoparticles in the droplet area. Figure 1 A is a regular droplet and inset shows the zoomed images of the marked areas and Figure 1 B shows the area of a droplet touched by a hydrophobic tip from the top of the droplet. It is clearly seen that the latex nanoparticles are uniformly assembled in the droplet area of the touched-droplet while arbitrary aggregates are observed in the case of normally drying droplet.

The influence of parameters such as tip and nanoparticle size, nanoparticle surface charge properties, and surface hydrophobicity on the assembly range and nanoparticle packing is discussed. The manipulation of the behavior of nanostructures in a droplet by other physical means is also demonstrated.

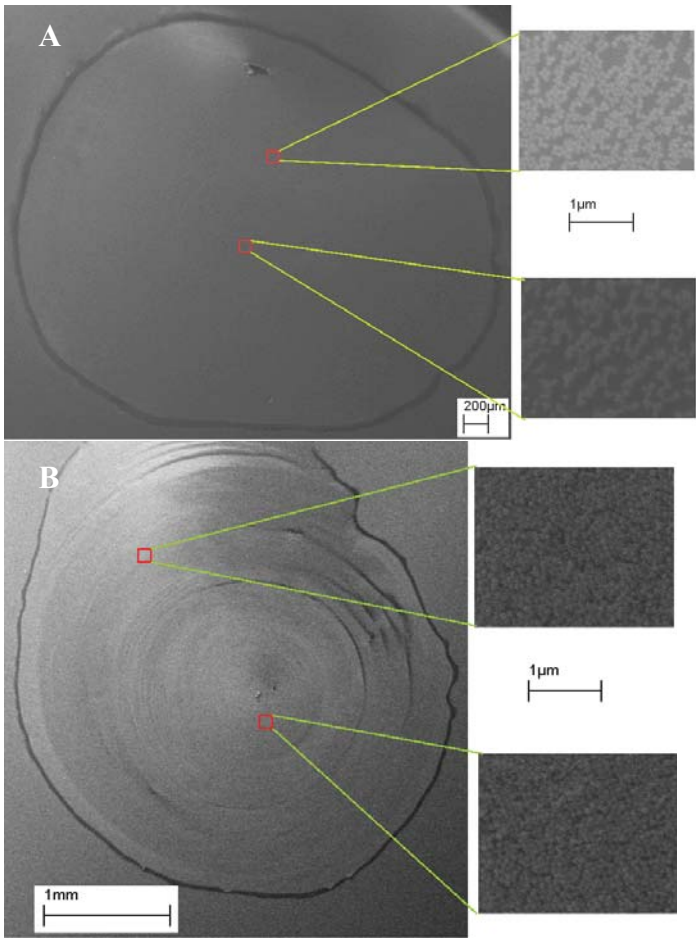

Figure 1. Assembly of 200 nm latex nanoparticles from a drying droplet on hydrophobic surfaces (A) and uniform assembly of the same latex nanoparticles upon touching on top of the droplet during its drying (B).

This work was supported by TUBITAK under Grant No. TBAG-108T605 and Yeditepe University.

*Corresponding author: mculha@yeditepe.edu.tr

[1] Mustafa Çulha., Self-Assembly of Nanostructures in Recent Advances in Nanoscience and Technology, Eds Sunil Kumar Bajpai / Murali Mohan Yallapu, PP 53-65, 2009 Bentham Science Publishers Ltd.
[2] Xia, D.; Li, D.; Luo, Y.; Brueck, S. R. J.; Adv. Mater., 18, 930, 2(006).
[3] Maye, M. M.; Nykypanchuk, D.; van der Lelie, D.; Gang, O. Small, 3, 10, 1678 (2007).

Surface Induced Asymmetry of Acceptor Wave Functions

Cem Çelebi

Faculty of Engineering and Natural Sciences, Sabanci University, 34956, Istanbul, Turkey

Abstract- Measurements of the local density of states of individual acceptors in III–V semiconductors show that the symmetry of the acceptor states strongly depends on the depth of the atom below a (110) surface. Tight-binding calculations performed for uniformly strained bulk materials demonstrate that strain induced by the surface relaxation is responsible for the observed depth-dependent symmetry breaking of acceptor wave functions. As this effect is strongest for weakly bound acceptors, it explains within a unified approach the commonly observed triangular shapes of shallow acceptors and the crosslike shapes of deeply bound acceptor states in III–V materials.

Dopant atoms are essential components in semiconductors not only because they provide extrinsic charges or magnetic moments, but because single dopants offer the potential to be used as the functional parts of nanoscale or quantum information devices. In order to utilize single dopants in such devices, their electronic and magnetic properties have to be understood in detail.

In the past decade many groups have scrutinized at the atomic scale the electronic and spectroscopic details of individual impurities, such as Si, Zn, and Mn, embedded in the topmost layers of a cleaved semiconductor crystal like GaAs or InAs [1-5]. A correct interpretation of these atomistic properties is essential for a proper understanding of the macroscopic properties of doped materials. For example, present models of impurity band formation and ferromagnetism in GaMnAs require a proper description of the atomic scale properties of individual Mn acceptors. The surface, however, is known to strongly influence the properties of an impurity close to the surface, and thus a central question for all such surface measurements via Scanning Tunneling Microscopy (STM) is how closely the local density of states (LDOS) is related to the properties of an impurity in the bulk.

In STM measurements, donors like Si in GaAs appear as highly symmetric isotropic round protrusions [1]. This picture of donors is in analogy with the hydrogenic impurity model. Unlike donors, shallow acceptors like Zn in GaAs and deep acceptors like Mn in GaAs appear as highly anisotropic triangular or cross-like contrast in STM measurements, respectively [2-5].

Here we report measurements and calculations for the LDOS of Mn acceptors in GaAs as a function of their distance below the reconstructed surface. We show that the STM contrast can be fully understood from the wave function of the impurity state itself. The shape of the hole distribution around the Mn acceptor for different dopant depths under the surface is analyzed at the atomic scale by using STM (Figure 1). We found that the acceptors located within the first ten subsurface layers of the semiconductor show a lower symmetry than expected from theoretical predictions of the bulk acceptor wave function [2,7]. They exhibit a strong (001) mirror asymmetry in STM measurements. The degree of acceptor wave function asymmetry was found to depend on the depth of the acceptor atom below the surface. The experimentally observed depth dependent change of the acceptor wave function symmetry was characterized quantitatively and interpreted successfully by tight-binding (TB) theoretical calculations. We were able to show within the TB model that, without a detailed description of the reconstruction of the near surface layers, the strain due to the relative displacement in between the surface and near surface atoms is responsible for the experimentally observed reduction of the bulk acceptor wave function symmetry. As this effect is strongest for weakly bound acceptors due to their smaller binding energies, it explains within a unified approach the commonly observed triangular shapes of shallow acceptors and the cross-like shapes of deeply bound acceptor states in III–V semiconductors.

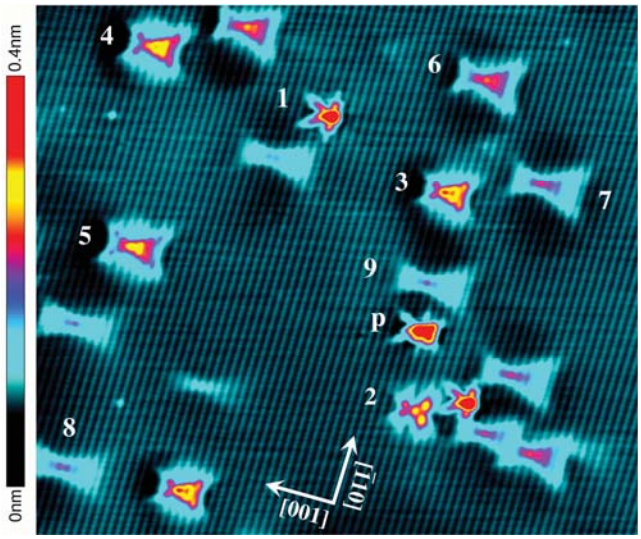

Figure 1: (45nm x 35nm) Constant-current STM topography image of the GaAs(110) surface showing a number of Mn acceptors in their neutral charge state. The numbers correspond with the atomic layer position of the Mn acceptors on and below the GaAs cleaved surface.

Corresponding author: cemcelebi@sabanciuniv.edu

[1] J. F. Zheng *et al*., Phys. Rev. Lett. **72**, 1490 (1994)
[2] A. M. Yakunin *et al*., Phys. Rev. Lett. **92**, 216806 (2004)
[3] F. Marczinowski *et al*., Phys. Rev. Lett. **99**, 157202 (2007)
[4] R. de Kort *et al*., Phys. Rev. B **63**, 125336 (2001)
[5] C. Çelebi *et al*., Phys. Rev. B **77**, 075328 (2008)
[6] C. Çelebi *et al*., Phys. Rev. Lett **104**, 086404 (2010)
[7] J.-M. Tang and M. E. Flatté, Phys. Rev. B **72**, 161315 (2005)

Charge Separation in Ruthenium Dyes Adsorbed on Nanoporous TiO_2 Layers

Cigdem Sahin[1,2], Thomas Dittrich[3], Canan Varlikli[1]*, Siddik Icli[1]
[1]*Solar Energy Institute, Ege University, 35100 – Bornova, Izmir, TURKEY*
[2]*Chemistry Department, Art & Science Faculty, Pamukkale University, Denizli, TURKEY*
[3]*Helmholtz Centre Berlin for Materials and Energy, Glienicker Str. 100, 14109 Berlin, GERMANY*

Abstract-The charge separation and electron back transfer process of some synthesized ruthenium dyes adsorbed on TiO_2 have been investigated by surface photovoltage spectroscopy under steady state and chopped illumination of Kelvin probe and capacitor arrangement, respectively. Differences in chelating behaviour of bpy-py and bpy-bpy complexes has found to have an effect on the electron back transfer proces

For the past two decades, polypyridyl ruthenium (II) complexes have been widely studied in dye sensitized solar cell (DSSC) [1]. These structures provide an attractive approach in controlling the charge separation, and recombination dynamics at the molecule/nanocrystal interfaces [2]. The understanding of the charge transport, charge separation, and recombination in the nanostructured materials is important for the development of an efficient dye sensitized solar cell.

The surface photovoltage spectroscopy is a contactless, non-destructive and sensitive technique for inorganic and organic semiconductor characterization [3]. This metod can provide information about surface and interface band bending, band gap, life time, carrier diffusion length, charge separation in bulk materials and thin films [3, 4].

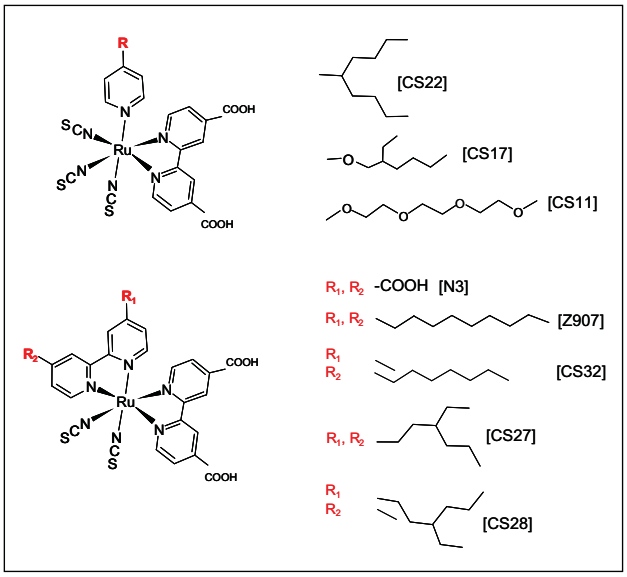

Figure 1. Structures of ruthenium (II) complexes [5].

In this work, ruthenium (II) complexes containing pyridine and bipyridine ligands (Figure 1) were synthesized according to literature [5]. Chelating effect in Ru dye molecules containing pyridine and bipyridine ligands adsorbed on ultra-thin nanoporous TiO_2 layers on charge separation and electron back transfer has been investigated by surface photovoltage spectroscopy (SPS) in argon atmosphere. The surface photovoltage were analyzed
under steady state and chopped illumination of Kelvin probe and capacitor arrangement, respectively.

We investigated contact potential differences (CPD) in Ru dye molecules adsorbed on nanoporous TiO_2 layers by Kelvin probe. The contact potential decreases starting at photon energies larger than 1.5 eV due to electron injection from dye molecules into the TiO_2.

The data obtained on electron back transfer process of ruthenium complexes that contain bpy-py and bpy-bpy ligands by the use of SPV has been reported in our previous study [5]. Here we report the data gained from Kelvin probe arrangement measurements and compare with the results obtained through SPV. Both of the technique used show that electron back transfer was practically not affected by branching or non-branching side groups in the bpy-bpy complexes. In contrast, electron back transfer was much less for bpy-py complexes in comparison to bpy-bpy complexes. This is attributed to chelating effect. Further, this result is supported with electrochemical properties of the ruthenium (II) complexes. These dyes are good alternative for nc-DSSC applications.

We acknowledge the project support funds of Ege University and Helmholtz Center Berlin (HZB) for Materials and Energy, the State Planning Organization of Turkey (DPT).

*Corresponding author e-mail: 1Tcanan.varlikli@ege.edu.tr

[1] K. Ocakoglu, F. Yakuphanoglu, J.R. Durrant, S. Icli, Solar Energy Materials & Solar Cells 92 (2008) 1047–1053.
[2] N. Hirata, J.J. Lagref, E.J. Palomares, J.R. Durrant, M.K. Nazeeruddin, M. Gratzel, D.D. Censo, Chem. Eur. J. 10 (2004) 595-602.
[3] L. Kronik, Y. Shapira, Surface photovoltage phenomena: theory, experiment and applications, Surface Science Reports 37 (1999) 1-206.
[4] M. Eschle, E. Moons, M. Gratzel, Optical Materials, 9 (1998) 138-144.
[5] C. Sahin, Th.Dittrich, C.Varlikli, S.Icli, M.Ch.Lux-Steiner, Solar EnergyMaterials&SolarCells, 94 (2010) 686–690.

Polypyrrole Grafting onto the Surface of Pyrrole Modified Silica Nanoparticles Prepared by One-step Synthesis

Abstract— The grafting of polypyrrole onto the surface of modified silica nanoparticles has been investigated. These silica nanoparticles were modified with pyrrole moieties prepared by Stober method in one-step starting from TEOS and a pyrrole-bearing trialkoxysilane compound. The effects of various reaction conditions, including reaction time, solvent, and molar ratio of water to alkoxy groups, have been investigated in order to obtain pyrrole-modified silica nanoparticles with the optimal core–shell structure and the smallest possible particle size. The grafting was carried out in aqueous $FeCl_3$ solution containing the modified silica nanoparticles, with pyrrole monomers. Several analytical tools have been employed to characterize the particles and to assess the degree of grafting, namely TEM, SEM, TGA, FTIR, and XPS. The final polypyrrole-grafted silica nanoparticles obtained had a mean diameter of about 220 nm and 50 wt.% of grafted polypyrrole with respect to the total weight of polypyrrole formed around the surface of the cores.

Polypyrrole (PPy) has been one of the most studied conductive polymers over several decades due to its outstanding properties, including environmental stability, anti-corrosion properties, redox properties, relatively high electrical conductivity, as well as ease of synthesis. However, similar to other kinds of substantially conductive polymers, its application has been limited due to unprocessability in terms of insolubility in common solvents and infusibility. Many attempts have been made to overcome the problem, including synthesis in emulsion or reverse emulsion systems using surface-active anions to increase the solubility [1, 2], blending with other polymers [3−8], and even preparation of PPy/clay embedded composite materials [9]. One of the employed approaches has been to reduce the size of the PPy particles to the micro- or nanoscale by polymerizing pyrrole in the presence of nanostructured materials, such as silica nanoparticles. Previously, we have described the preparation of PPy-coated silica nanoparticles by *in situ* polymerization of pyrrole in the presence of vinyl-modified silica nanoparticles [10]. The latter had been synthesized by a one-step method starting from tetraethoxysilane (TEOS) and vinyltriethoxysilane (VTEOS) [11]. The most important outcome of the work [10] was to obtain PPy–silica nanoparticles with a core–shell structure having a smooth and solid PPy shell of thickness ~7 nm, in contrast to the raspberry-like morphology observed by other investigators [12].

In the present work, in order to synthesize Py-modified silica nanoparticles, *N*-(3-(trimethoxysilyl)propyl)pyrrole (TMSPP) was added to the reaction vessel as an alkoxysilane modifier bearing a pyrolle ring at one end, during the course of the reaction with TEOS. The reaction conditions were tuned so as to obtain the desired Py-modified silica nanoparticles in terms of size and shell structure. PPy grafting was then achieved by *in situ* polymerization of pyrrole in the presence of Py-modified silica nanoparticles in an aqueous solution of $FeCl_3$. The resulting core–shell particles were characterized by TEM, SEM, FTIR, TGA, and XPS.

We have examined different reaction parameters including solvent (EtOH or MeOH), reaction time, water/alkoxide molar ratio, in order to obtain the possible smallest particle with well defined shell structure of the pyrrole moiety on the surface of the silica nanoparticles and PPy shell on the final PPy-grafted nanoparticles. Narrowly distributed particles with average size about 200 nm with 26 nm thick shell of Py moiety can be obtained using methanol as the solvent, a reaction time of 90 min, and a water/alkoxide group molar ratio of 20:1. *In situ* PPy grafting was accomplished using the Py-modified silica nanoparticles in the presence of excess pyrrole monomer, afforded PPy grafted silica nanoparticles with with raspberry like morphology, as evidenced by TEM and XPS results. A directly grafted PPy fraction of about 50% of the overall PPy was estimated using TGA studies. Figure 1 presents TEM images for the Py modified silica nanoparticles obtained in different reaction time of the one-step method in EtOH and Figure 2 shows TEM images for the final PPy-grafted silica nanoparticles after optimization of the reaction parameters.

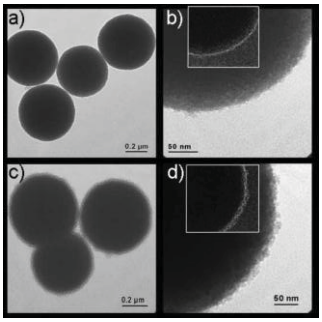

Figure 1: TEM images showing the particles obtained in EtOH at 40 °C in different magnification levels; (a) and (b): after 30 min of reaction, (c) and (d): after 90 min. Inset figures are '*find edge*' processed images to revel the differences in surface of the particles upon reaction time.

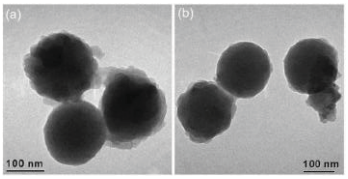

Figure 2: TEM images of PPy-grafted silica nanoparticles on a) Py silica nanoparticles prepared after 30 min and b) after 90 min of reaction.

* Corresponding author: pourabas@sut.ac.ir

Boron-Dipyrrins as Photosensitizers for Dye-Sensitized Solar Cells

Engin U. Akkaya[1,2]*
[1]Department of Chemistry, Bilkent University, Ankara 06800, Turkey
[2]UNAM-Institute of Materials Science and Nanotechnology, Bilkent University, Ankara 06800, Turkey

Abstract-We initiated a synthesis program aiming long wavelength absorbing sensitizers for DSSC. These Boron-dipyrrin based sensitizers had the largest conversion efficiencies beyond 750 nm.

Dye-sensitized solar cells [1] (DSSCs) are promising alternatives to more expensive solar cell technologies. However, stringent optimization of every component in a DSSC assembly is clearly needed. The sensitizer dye is of course an important component of the system. Optimal dye, requires an understanding of myriad of processes. Rational design of solution phase behavior is an attainable goal. However, in condensed phases, films, or on surfaces, the "rational design" of properties encounters formidable challenges. Our research group has been involved in the chemistry and applications of Boron-dipyrrin (a.k.a., BODIPY, BDP, boradiazaindacene, etc.) class of dyes for the last decade. As a class of chromophores, Boron-dipyrrin dyes are highly attractive because of their high quantum yield, large extinction coefficients, good photostability and rich chemistry. We realized that Boron-dipyrrin structure should lead to significant electronic charge reorganization following excitation, and by proper functionalization, this charge separation could be exploited.

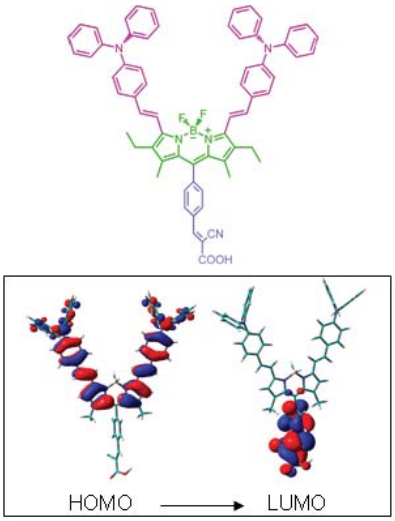

Figure 1. Frontier orbitals, showing electronic reorganization following a HOMO-LUMO transition.

DFT calculations for the dye 2, at the B3PW91/6-31+G(d,p)//B3LYP/6-31G(d) level of the theory, support directional movement of charge on excitation.[3] The HOMO is primarily comprised of π framework of the BODIPY and the styryl groups, with significant contributions from π electrons of the diphenylamino substituent; whereas the LUMO is very clearly confined to the π-system of the anchor group. This overall picture, found at all levels considered, shows a very clear electron density shift from the π framework of BODIPY core and the styryl substituents to the pendant carboxyphenyl moiety upon a vertical excitation of the π - π* type.

Encouraged by the theoretical insight, we synthesized a series of long wavelength absorbing Boron-dipyrrin dyes targeting especially the red and near-IR region of the solar spectrum. Most of the compounds we synthesized showed a plateau of efficiency between 400-800 nm. While the overall conversion efficiency (η) is around 2 %, these dyes were very effective in the red to near-IR region, better than widely known Ruthenium complexes.

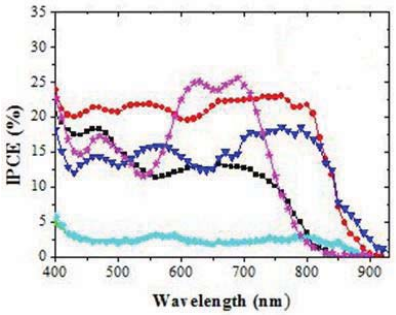

Figure 2. ICPE vs. wavelength data for the series of dyes investigated as a part of this work.

TiO_2 sensitized device (with liquid electrolyte) construction and all efficiency calculations were obtained in a collaborative work with Prof. Dr. M. Gratzel and Dr. S. M. Zakeeruddin in EPFL, Switzerland.
Our recent progress will be discussed highlighting the structure activity-correlations, or lack thereof.

*Corresponding author: eua@fen.bilkent.edu.tr

[1] (a) Oregan, B.; Gratzel, M. Nature 1991, **353**, 737–740. (b) Hagfeldt, A.; Gratzel, M Acc. Chem. Res. 2000, **33**, 269–277.
[2] M. K. Nazeeruddin, P. Pechy, T. Renouard, S. M. Zakeeruddin, R. Humphry-Baker, P. Comte, P. Liska, L. Cevey, E. Costa, V.Shklover, L. Spiccia, G. B. Deacon, C. A. Bignozzi, M. Gratzel, J. Am. Chem. Soc. 2001, 123, 1613.
[3] (a) S. Erten-Ela, M. D. Yilmaz, B. Icli, Y. Dede, S. Icli and E. U. Akkaya, Org. Lett., 2008, **10**, 3299 (b) Rousseau, T.; Cravino, A.; Bura,T.; Ulrich, G.; Ziessel, R.; Roncali, J.; Chem.Comm. 2009, 1673-1675.

Conjugated Polymer Solar Cells and Their Nanostructural Improvement

Serap Gunes[1*], Emel Cevik[1], Derya Ilicali[1], Gulay Gunday[1], Ismail Karatas[1], Adem Karsli[1], Andreas Wild[2], Daniel Ayuk Mbi Egbe[3], Nimet Yilmaz Canli[1], Öznur Yasa[4], Belkıs Bilgin Eran[4], Niyazi Serdar Sariciftci[3]

[1] *Yildiz Technical University, Faculty of Arts and Science, Dept of Physics, Davutpasa Campus, 34210, Esenler/ISTANBUL/TURKEY*
[2] *Laboratory of Organic and Macromolecular Chemistry, Friedrich-Schiller-University Jena, Humboldtstr.10, D-07743 Jena, Germany.*
[3] *Linz Institute for Organic Solar Cells (LIOS), Johannes Kepler University Linz, Physical Chemistry, Altenberger Strasse 69, A-4040 Linz/Austria*
[4] *Yildiz Technical University, Fac. Of Arts and Science, Dept of Chemistry, Davutpasa Campus, 34210, Esenler/Istanbul/Turkey*

Abstract-In this study, an overview of our recent results on the performance of the organic solar cells employing thiophene and anthracene based polymers and also, the effect of addition of liquid crystals into the performance of organic solar cells using poly(3-hexylthiophene) (P3HT) and a fullerene derivative (1-(3-methoxycarbonyl) propyl-1-phenyl[6,6]C_{61}) (PCBM) will be presented. The routes for possible nanostructural improvement will be discussed.

A solar cell converts sunlight into electricity. Global warming, limited fossil fuel resources and growing world energy demand encourages researchers to investigate new routes for viable renewable energy sources. Solar energy is clean, abundant and is for free. Inorganic solar cell device technology exhibited power conversion efficiencies over 20 % [1]. Although they reached high efficiencies, these technologies are too expensive to be competitive on a global scale. Therefore, recently researchers focus on new, cheap alternatives for conventional inorganic solar cells. The organic, polymer based photovoltaic elements have introduced the potential of obtaining a cheap and easy method to produce energy from light [2]. The material properties of organic semiconducting materials (conjugated polymers) can be chemically manipulated with a variety of easy and cheap processing techniques [3].

The optimum overall performance of a polymer solar cell can be achieved via balancing the various requirements on light absorption, photogeneration, transport and extraction of charge carriers [4]. Recently, the power conversion efficiencies over 6 % have been reported for organic solar cells [5,6]. However, this value has to be improved to be competitive with the conventional solar cells. On the other hand, there is a considerable progress in the evolution of organic solar cells from pure scientific research to a possible industrial application. Recent efforts are devoted to the investigation of operating mechanisms, new synthesis routes, new device architectures, stability of the organic materials, life time and encapsulation.

Among the various schemes of device structure, bulk heterojunction (BHJ) has been the most widely employed for polymer solar cells. The interpenetrating network of blended electron donor and acceptor materials provides a large interface between the two materials, allowing significant exciton separation and carrier transport to the respective electrodes [7].

In this study, an overview of our recent results on the organic solar cells employing thiophene and anthracene based polymers and also, the effect of addition of liquid crystals into the performance of organic solar cells using poly(3-hexylthiophene) (P3HT) and a fullerene derivative (1-(3-methoxycarbonyl) propyl-1-phenyl[6,6]C_{61}) (PCBM) will be presented. The routes for possible nanostructural improvement will be discussed. We achieved efficiencies up to 1.8 % for organic solar cells comprising of thiophene based conjugated polymers and PCBM [8]. We also achieved efficiencies up to 2.6 % **1T**using chiral (S)-5-octyloxy-2-[{4-(2-methylbuthoxy)-phenylimino}-methyl]-phenol liquid crystalline compound as additive into polymer solar cells [9].

*Corresponding Author: sgunes@yildiz.edu.tr

[1] M A Green, K Emery, D L King, S Igari, W, Warta Progress in Photovoltaics Research and Application 9, 287 (2001)
[2] N. S Sariciftci, L.Smilowitz, A. J. Heeger, F.Wudl Science 258, 1474 (1992)
[3] H. Spangaard, F. Krebs Sol. Energy Mat. Sol. Cells 83, 125 (2004)
[4] D. Chirvaze, J. Parisi, J.C. Hummelen, V. Dyakonov Nanotechnology 15, 1317 (2004)
[5] S. H. Park, A. Roy, S. Beaupre et al Nature Photonics 3, 297, (2009)
[6] H.-Y Chen, J.Hou, S. Zhang, Y. Liang, G..Yang , Y. Yang, L.Yu, Y. Wu, G.Li, Nature Photonics 3, 649, (2009)
[7] J. H. Huang, Z-Yo Ho, D. Kekuda et al Nanotechnology,20, 025202, (2009)
[8] S. Gunes, A. Wild, E. Cevik, A. Pivrikas, U. Schubert, D. Egbe, Solar Energy Materials and Solar Cells 94, 484, (2010)
[9] N. Yilmaz Canli, S. Gunes, A. Pivrikas, A. Fuchsbauer, D. Sinwel, N. S. Sariciftci, O. Yasa, B. Bilgin Eran, Solar Energy Materials and Solar Cells, in press

Photo-responsive n-channel organic field effect transistor based on naphthalene bis-benzimidazole with divinyltetramethyl disiloxane-bis (benzo-cyclobutene) gate insulator

Siddik Icli[1], Cem Tozlu[1,2] Sule Erten-Ela[1]
[1]Solar Energy Institute, Ege University, Bornova, 35100 Izmir, Turkey
[2]Physics Department, Art and Science Faculty, Mugla University, 48000 Mugla, Turkey

Abstract— A n-channel photoresponsive organic field effect transistor (photOFET) based on naphthalene bis-benzimidazole (NBBI) with improvement responsitivity by employing a transparent divinyltetramethyl disiloxane-bi (BCB) as dielectric is presented. The NBBI based organic field effect transistor exhibited saturated electron mobility of 6×10^{-3} $cm^2/V.s$ with threshold voltage of 7.2 V. The photosensitivity and photoresponsivity of device are found to be 93.4 and 14.3 mA/W, respectively at off-state of device under white light at A.M 1.5 condition.

The derivatives of naphthalene tetracarboxylic organic semiconductors are planar, chemically robust and redox-active compounds. Three-terminal phototransistor is a key component for light detection and photoswitching in an optoelectronic circuit [1]. Several groups have reported photoresponsive organic field effect transistor (photo-OFET) based on polymer or organic semiconductors, such as poly(3-octylthiophene) [2], pentacene [3]. Naphthalene tetracarboxylic dianhyride (NTCDA) and naphthalene tetracarboxylic dimide (NTCDI) derivatives with electron-withdrawing groups, such as fluoroalkyl, fluorinated phenyl, cyano etc. have been developed to improve air stability and mobility of thin film transistor [4].

We have prepared naphthalene bis benzimidazole (NBBI) thin-film transistor with top contact/bottom gate geometry in order to sense visible light as shown in Fig.1. The soluble dielectric that is divinyltetramethyl disiloxane-bis (benzo-cyclobutene) (BCB) was used to obtain high transparency of dielectric on indium tin oxide (ITO) to penetrate light through the device. The photosensing characteristics of NBBI based field effect transistor are investigated under different illumination intensities of visible light. UV-Vis spectra of NBBI semiconductor for solution phase and solid phase ws investigated. The absorption of naphthalene bis-benzimidazole shifts the visible region in the range of 350–600 nm according to solution phase. Fig. 2 (a) shows output characteristics of NBBI field effect transistor fabricated on top of the BCB gate-insulator with Al top drain-source contacts in dark. The drain current I_{ds} increases almost linearly with V_{ds} implies that good establishment of ohmic contact between NBBI semiconductor and Al contacts. This suggests that electron accumulation mode is achieved in the channel that is formed at the dielectric-active layer interface under different positive gate voltages, V_{gs}, applied to ITO glass substrate.

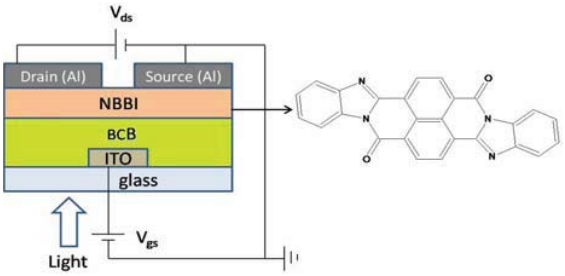

Figure 1. Cross section of device and chemical structure of NBBI.

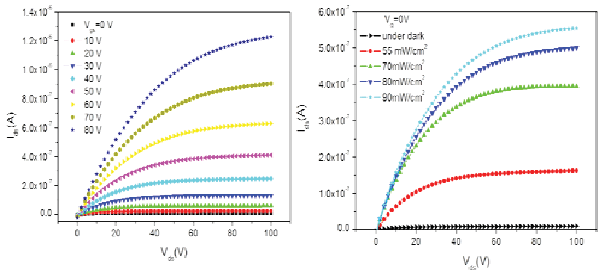

(a) (b)

Figure 2. The output characteristics of NBBI based photOFET in dark (a) and under illumination at V_{gs} = 0V (b).

A photo-induced charge carrier generation is clearly observed with increase of the drain-source current depend on illumination intensity without gate induced. This indicates that light behaves forth terminal that optically switches on/off device in addition to conventional source, drain and gate terminals as seen clearly in Fig. 2 (b). The NBBI semiconductor shows good photo-responsive field effect transistor characteristics with respect to white light.

The photosensitivity is defined as ratio photocurrent to dark current (I_{ph}/I_{dark}). The photosensitivity of device was found to be 1.82 in turn-on state (V_{gs} = 80V) and 93.4 (V_{gs} = 0V) in turn-off state, respectively at the illumination intensity of 90 mW/cm^2 in accumulation regime. When the device in depletion mode i.e. turn-off state ($V_{gs}<V_{th}$), the photocurrent is the directly proportional to incident light power (P_{inc}). Therefore photo-generated charge carriers increase channel conductivity and the drain-source current that leads to the high photosensitivity at turn-off state of device [5]. The photosensitivity of the studied transistor based on NBBI semiconductor is competitive with pentacene thin film transistors fabricated on poly-4-vinylphenol gate dielectrics and MEH-PPV (poly(2-methoxy-5-(2'-ethyl-hexyloxy)-1,4-phenylenevinylene)) fabricated on SiO_2 [6-7].

*Corresponding author: s_icli@yahoo.com

[1] S. M. Sze, Physics of Semiconductor Devices, third ed., Wiley, New York, 2007.
[2] K.S. Narayan, N. Kumar, Appl. Phys. Lett. **79**, 1891-1893 (2001).
[3] S. Okur, F. Yakuphanoglu, E. Stathatos, Microelec. Engin. **87**, 635-640 (2010).
[4] K. C. See, C. Landis, A. Sarjeant, H. E. Katz, Chem. Mater. **20**, 3609-3616 (2008).
[5] C.S. Choi, H.S. Kang, W.Y. Choi, D.H. Kim, K. S. Seo, IEEE Microwave Theory and Tech. **53,** 256-263 (2005).
[6] J. H. Kwon, M. H. Chung, T.Y. Oh, H. S. Bae, J.H Park, B. K. Ju, F. Yakuphanoglu, Sensor Actuat. A **156**, 312–316 (2009).
[7] Y.R. Liu, J.B. Peng, P.T. Lai, Thin Solid Films **516**, 4295-4300 (2008).

Effect of the SAM layer on the Electrical Characteristics and Interface Properties of the ITO/SAM/TPD/Al Schottky Diode

Ali Kemal Havare,[1] Salih Okur,[2]* Nesli Yagmurcukardes[2], Hasan Aydın[2], Mustafa Can[1] and Serafettin Demic[1],
[2]*Izmir Institute of Technology, Faculty of Science, Department of Physics Gülbahce Koyu Kampüsü, Urla, Izmir, 35430, Turkey*
[1]*Ege University, Institute of Solar Energy, Bornova, 35100 Izmir, Turkey*

Abstract-The electrical characteristics of the ITO/TPD/Al and ITO/SAM (THIBSi)/TPD/Al Schottky diodes have been investigated by current–voltage (I–V) characteristics. We used new SAM molecules to construct ITO/SAM/TPD/Al Schottky devices, and studied the influence on charge tunneling. An ideality factor higher than unity can result from the interface state. The ideality factor n and barrier height ϕ_b values of the ITO/TPD/Al and ITO/SAM (THIBSi)/TPD/Al diode were found to be 1.24 and 0.85 eV, 1.28 and 0.40 eV, respectively. The barrier height of the diode was determined from I–V characteristics.

The device performance of a Schottky diode depends on electrical and electronic characteristics of the metal/organic Semiconductor junction [1]. Therefore, the understanding of electronic properties of the interface between metal and organic semiconductors is important for organometalic device applications [2, 3]. The electronic parameters and interface properties of the ITO/TPD/Al and ITO/SAM (THIBSi)/TPD/Al Schottky diodes have been investigated by current-voltage characteristics.

In this study, Schottky energy barrier was constituted between metal and organic material. Schottky contact exhibits a reproducible rectifying behavior and the I–V characteristics are well explained by the conventional Schottky-barrier junction model. The electronic parameters of the diode such as ideality factor and barrier height are compared with ITO/Al, ITO/TPD/Al and ITO/SAM (THIBSi)/TPD/Al. We have synthesized (4'-iodobifenil-4-il) trihidroksisilan (THIBSi) for organic semiconductors as SAM layer. Fig.1 shows the structure of the SAM molecule and Schottky diode.

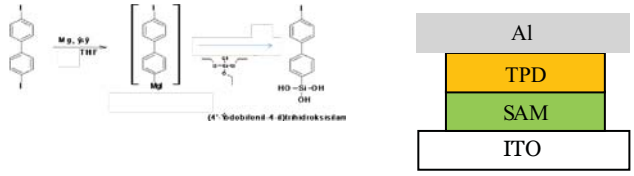

Figure 1. Synthesis of SAM molecule and Structure of Schottky diode

Schottky diode was prepared with self-assembly monolayer (SAM) technique. We prepared 1mM THIBSi SAM solutions with chloroform. ITO were kept in the solutions for two days to be formed the SAM film, and then rinsed and dried. After that TPD was evaporated to constitute 50 nm thin film. Finally 200 nm Al was formed as a top contact.

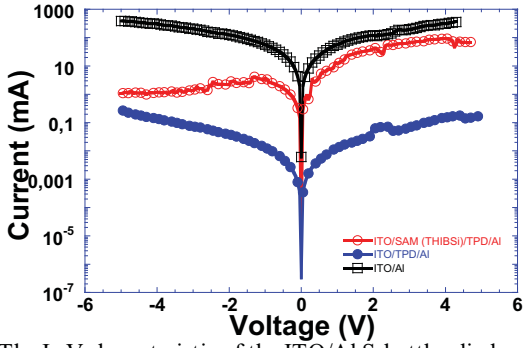

Figure 2. The I- V characteristic of the ITO/Al Schottky diode.

The I–V characteristics of the ITO/SAM (THIBSi)/TPD/Al Schottky contact are shown in Fig. 2. It shows that the SAM layer enhances the charge tunneling in ITO/SAM (THIBSi)/TPD/Al with respect to ITO/TPD/Al diode. Electronic parameters such as ideality factor, barrier height of ITO/SAM (THIBSi)/TPD/Al Schottky junction have been investigated by relation;

$$I = AA^*T^2 \exp\left(-\frac{q\Phi_b}{kT}\right)\exp\left(\frac{qV}{nkT}\right)\left[1-\exp\left(-\frac{qV}{kT}\right)\right] \quad (1)$$

where n is the ideality factor, A is the contact area, T is the temperature, A* is the Richardson constant, q is the electronic charge, k is Boltzmann constant, and ϕ_b is the barrier height.

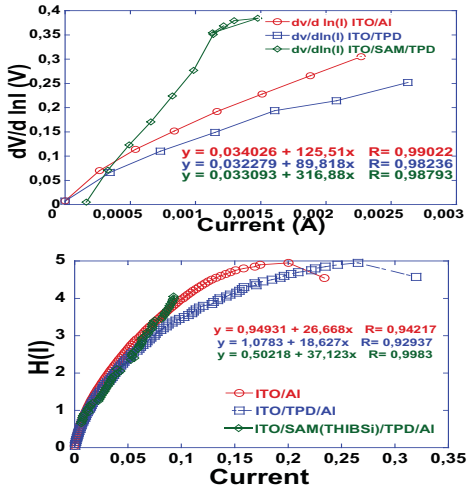

Figure 3. The plots of dV/dln (I) - I and H (I) - I of the ITO/Al Schottky diode

The series resistance can be evaluated using a method developed by Cheung [4] to determine the barrier height, ideality factor, and series resistance. Cheung's functions are defined as,

$$\frac{dV}{d\ln I} = n\frac{kT}{q} + IR_s \quad (2)$$

$$H(I) = V - n\frac{kT}{q}\ln\left(\frac{I}{AA^*T^2}\right) = H(I) = IR_s + n\Phi_b \quad (3)$$

The plots of dV/dln (I) - I and H (I) - I are shown in Fig. 3. The diode shows a nonideal current-voltage behavior due to higher than unity. The n values were obtained from the intercept of dV/dln (I) - I plot for ITO/TPD/Al and ITO/SAM (THIBSi)/TPD/Al, respectively and were found to be 1.24 and 1.28. The ϕ_b and R_s values were calculated from the H (I) - I plot using the obtained were found to be 0.85 eV and 0.40 eV and 18 kΩ 37 kΩ, respectively. This work was supported by TUBITAK under Grant No. TBAG-108T718.

*Corresponding author: salihokur@iyte.edu.tr

[1] Willander, M.; Assadi, A.; Svensson, C. Synth. Met. 1993, 55, 4099
[2]Fahrettin YakuphanogluJ. Phys. Chem. C 2007, 111, 1505 1507
[3] F. Yakuphanoglu, S. Okur, H.Özgener Mic. Eng. 86 (2009) 2358
[4] Cheung, S. K.; Cheung, N. W. Appl. Phys. Lett. 1986, 49, 85.

Structural and Electronic Investigation of Pentacene Thin Films on Flat and Stepped Ag(111) Surfaces

Mehmet Fatih Danışman[1], Ersen Mete[2], Berrin Özkan[1], İlker Demiroğlu[1], Şinasi Ellialtıoğlu[3]
[1] *Department of Chemistry, Middle East Technical University, Ankara 06531, Turkey*
[2] *Deparment of Physics, Balikesir University, Balikesir 10145, Turkey*
[3] *Department of Physics, Middle East Technical University, Ankara 06531, Turkey*

Abstract-Here we present a theoretical and experimental study of the structural profiles and electronic properties of pentacene multilayers on Ag(111) surfaces. We have performed first-principle total energy calculations based on the projector-augmented wave method within the density functional theory (DFT) framework to investigate the initial growth patterns of pentacene on flat and stepped Ag(111) surfaces. In addition structure of pentacene thin films grown by supersonic molecular beam deposition has been studied as a function of surface step density (by using vicinal and precisely tilted surfaces) and pentacene kinetic energy, systematically, by means of time of flight and helium diffraction measurements. Both experimental and theoretical results suggest that step edges can trap the pentacene molecules and act as nucleation sites for the growth of ordered thin films with a crystal structure similar to that of bulk pentacene. DFT calculations show that due to relatively weak interaction of the pentacene monolayer and the silver surface, upon growth of second and higher layers, the monolayer configuration changes slightly in agreement with the experimental results where upon desorption of pentacene multilayers a new monolayer phase was observed.

Pentacene thin films are the subject of extensive research efforts due to (a) their uses in organic electronic applications such as this film transistors and (b) being a model system for studying aromatic molecule – metal surface interactions. The electronic and crystal structure and growth mechanism of pentacene thin films on Ag(111) surface is still a matter of debate. To help resolve the contradictory issues in the literature we have performed both computational and experimental studies on this system.

In our experimental studies we have found that an ordered multilayer pentacene film that resembles the bulk crystal can be formed at low substrate temperatures (200K) by using supersonic molecular beam only on a stepped surface. When such a multilayer is desorbed by annealing the remaining pentacene monolayer shows a different crystal structure then that of the initially grown monolayer phase. This is shown in the helium diffraction spectra given below where the different peak intensities and positions for these two cases can clearly be seen.

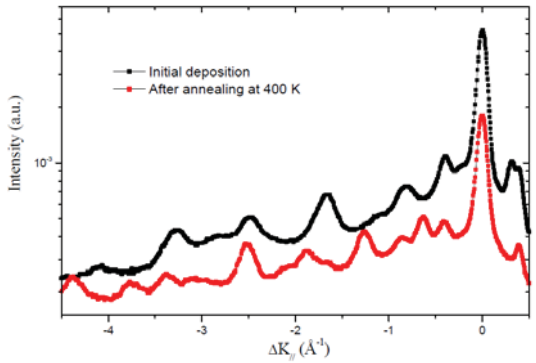

Figure 1. Diffraction scans of pentacene monolayers along <11-2> direction: Black curve shows the diffraction pattern immediately after one monolayer pentacene deposition on a stepped Ag(111) surface at 200 K substrate temperature by supersonic molecular beam deposition. The red curve shows the diffraction pattern obtained after annealing of pentacene multilayers, deposited at the same conditions as above, at 400 K. At this temperature multilayer desorbs and a new monolayer phase appears as indicated by the change in the diffraction pattern.

In our DFT studies we have found that adsorption energy of an isolated molecule increases at the step edge (0.615eV) and the minimum energy configuration is a tilted one resembling the experimentally determined pentacene geometry. In addition on the terrace there is an almost flat potential energy surface with weak pentacene adsorption energy (0.230 eV). These findings suggest that due to weak pentacene-surface interactions growth of multilayers may induce changes in the monolayer structure and the step edges can trap pentacene molecules in a tilted geometry which in turn may initiate the growth of a tilted multilayer structure as observed experimentally.

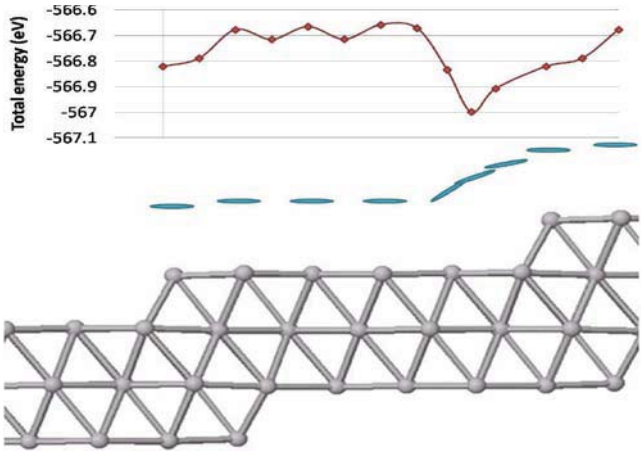

Figure 2. Energetical behaviour of pentacene molecule on Ag(233) surface.

Surface Patterning and Functionalisation for Nanotechnological Applications

Mustafa Ersoz

Selcuk University, Faculty of Science, Department of Chemistry, 42075 Konya, Turkey

Abstract- Topographical and/or chemical patterning of surfaces from the micrometer down to the nanometer length scale is frontier in a science with significant many attractive nano- and biotechnological applications such as for functionalisation of surfaces i.e, fundamental cell–surface interaction studies [1], advanced biosensors,[2], fabrication of DNA arrays on solid surfaces and so on. Surface patterning is a major route to the preparation of surface structures ordered at least in one lateral direction and mainly used for creation of novel materials and devices. In particular, substrate i.e, cell, protein, DNA–surface interaction studies it is imperative to control the topography and chemical surface functionality over the mentioned length scales simultaneously.[3]. Among the currently available approaches to obtain well-defined patterned substrates, one can differentiate i) massively parallel and ii) serial approaches. The former include conventional photolithography and more recently introduced technologies, such as microcontact printing (μCP) [4] and nano-imprint lithography (NIL),[5].

It has been demonstrated that microcontact printing (μCP) is becoming increasingly popular in terms of fast, inexpensive, simple, does neither require clean room instrumentation nor absolutely flat surfaces, plus it offers a way to create complex patterns particularly preparation of microarrays on surfaces even of sub-micrometer lateral dimensions. The printed arrays can be functionalized by using of various heterobifunctional structures. Originally, it was used to print self-assembled monolayers of alkanethiolates on gold or silanes on glass surfaces, then extended to stamp proteins, peptides or colloids on a variety of different surfaces to produce patterns of cells for different applications. The microcontact printing can be considered as a new potential technology platform to pattern the molecules on surfaces. The applicability of Microcontact printing (μCP) for functionalization of surfaces will be demonstrated for nanotechnological applications.

References

[1] J. Duvigneau, S. Cornelissen, N. B. Valls, H. Schonherr,and G. J. Vancso “Reactive Imprint Lithography: Combined Topographical Patterning and Chemical Surface Functionalization of Polystyrene-block-poly(tert-butyl acrylate) Films” Adv. Funct. Mater. 2010, 20, 460–468,

[2] a) P. Jonkheijm, D. Weinrich, H. Schro¨der, C. M. Niemeyer, H. Waldmann, “*Chemical Strategies for Generating Protein Biochips”* Angew. Chem. Int. Ed. 2008, 47, 9618. b) E. Phizicky, P. I. H. Bastiaens, H. Zhu, M. Snyder, S. Fields, “Protein analysis on a proteomic scale” Nature 2003, 422, 208.

[3] A. Embrechts, C. L. Feng, I. Bredebusch, C. E. Rommel, J. Schnekenburger, G. J. Vancso, H. Scho¨nherr, in Surface Design: Applications in Bioscience and Nanotechnology (Eds: R. Forch, H. Schonherr, A. T. A. Jenkins), Wiley-VCH, Weinheim, Germany 2009, p. 233.

[4] a) P.E. Dyer, S.M. Mawadi, C.D. Walton, M. Ersoz, P.D.I. Fletcher and V.N. Paunov, “157-nm laser micromachining of N-BK7 glass and replication for microcontact printing” *Appl. Phys. A. Mater. Sci. & Process.* 77, 391-394 (2003), b) C. Xu, P. Taylor, M. Ersoz, P.D.I. Fletcher, V.N. Paunov, “Microcontact Printing of DNA-Surfactant Arrays of Solid Substrates “J. Mat. Chem., 13, 3044-3048 (2003) c) G. Arslan, M. Özmen, İ. Hatay, İ.H. Gübbük, M. Ersöz “Microcontact Printing of an Alkylsilane Monolayer on the Surface of Glass” Turk. J. Chem., 32, 313-321, (2008)

[5] a) F. Johansson, P. Carlberg, N. Danielsen, L. Montelius, M. Kanje, “Axonal outgrowth on nano-imprinted patterns” Biomaterials 2006, 27, 1251 b) D. Falconnet, D. Pasqui, S. Park, R. Eckert, H. Schift, J. Gobrecht, R. Barbucci, M. Textor, “A Novel Approach to Produce Protein Nanopatterns by Combining Nanoimprint Lithography and Molecular Self-Assembly” Nano Lett. 2004, 4, 1909.

An electrochromic device studies of a novel spiro-fluorene bridging bicarbazole derivative

Ozlem Usluer[1,2], Sermet Koyuncu[3]*, Serafettin Demic[1]*, Siddik Icli[1], and René A.J. Janssen[4]
[1]*Solar Energy Institute, Ege University, 35100, Bornova, Izmir, Turkey*
[2]*Department of Chemistry, Mugla University, 48000, Mugla, Turkey*
[3]*Çan Vocational School, Çanakkale Onsekiz Mart University, 17400, Çanakkale, Turkey*
[4]*Molecular Materials and Nanosystems, Eindhoven University of Technology, Eindhoven, The Netherlands*

Abstract- A novel electroactive monomer, 2,7-bis(carbazol-9-yl)-9,9'-spiro(cyclododecane-1,9'-fluorene) (SFC) was synthesized and electropolymerized to give a very stable electrochromic polymer with a high contrast ratio (ΔT = 58% at 800 nm). An electrochromic device, assembled in the sandwich configuration (ITO-coated glass/anodically coloring polymer (poly-SFC)//gel electrolyte//cathodically coloring polymer (PEDOT)/ITO-coated glass), exhibited a short response time (about 1s), a high redox stability, and a high coloration efficiency (1377 $cm^2\ C^{-1}$).

Electrochromic conducting polymers have several advantages owing to a fast response time arising from their high conductivity and easy color tuning by controlling the effective π-conjugation length [1]. Spiro-functionalization at the bridge position of fluorene (C-9) having a specific steric configuration has been attracting attention as organic functional material in terms of its specific physical properties and their high photoluminescence (PL) and electroluminescence (EL) efficiencies and high thermal stabilities [2]. Besides, exploiting their intrinsic photophysical and redox properties, carbazole based compounds are studied in many applications such as electrochromic devices, organic light-emitting diodes, organic field-effect transistors and photovoltaic cells [3].

In this study, a novel electroactive monomer, **SFC** (2,7-bis(carbazol-9-yl)-9,9'-spiro(cyclododecane-1,9'-fluorene)), was synthesized in four steps. The chemical structure of SFC was elucidated from its FT-IR, ^1H&^{13}C-NMR, and MALDI-ToF data. (Figure 1).

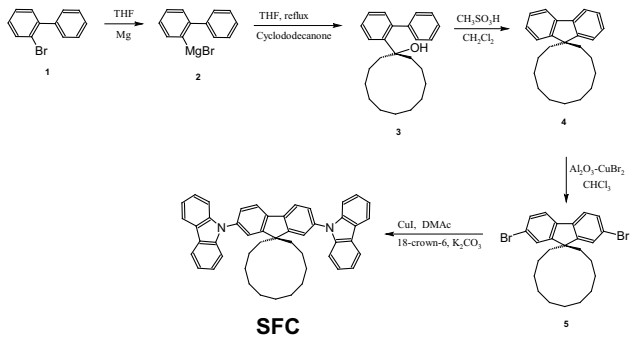

Figure 1. Synthetic route to SFC.

The electroactive polymer obtained by repetitive cycling at a potential between 0.0V and +1.6V (potentiodynamic method), exhibited two reversible waves at 1.14-1.25 and 1.35-1.46V (Figure 2).

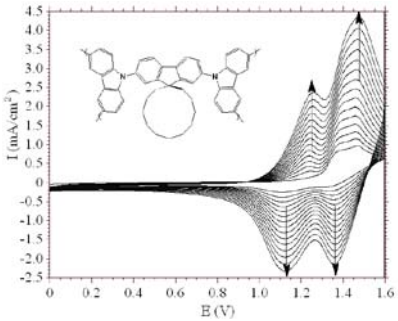

Figure 2. Repeated potential scanning of SFC monomer

During the scanning process, the peak at 448 nm initially intensified (<+1.2V) and then dramatically diminished at higher potentials (>+1.2V). Furthermore, first and second broad bands intensified at 972 (0.0–+1.4V) and 800 nm (+1.4–2.0V) indicated the formation of polarons and bipolarons on poly-SFC film, respectively (Fig. 2). During the oxidation process, the transparent film with CIE color parameters *(Luminance L = 91, hue a = -8, and saturation b = 5)* turned into yellowish green *(L: 87; a:-59; b: 83),* green (*L:45; a:-46; b:42*) and then dark green *(L:16; a:-21; b:11)*, respectively (Figure 3). Furthermore, the optical contrast (*ΔT*%) measured as the difference between neutral and oxidized states were found to be 58% at 800 nm.

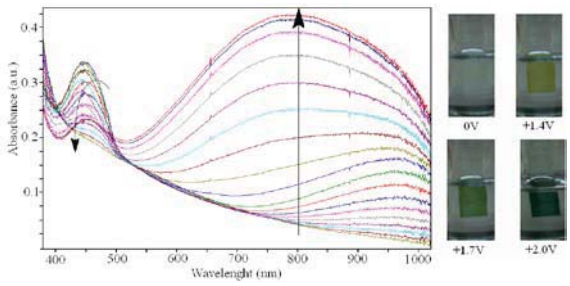

Figure 3. Spectro-electrochemical measurements and color changes of poly-SFC film between 0.0-2.0V.

The electrochromic device (ECD) was assembled in a sandwich cell configuration: ITO coated glass/anodically coloring polymer (poly-SFC)//gel electrolyte//cathodically coloring polymer (PEDOT)/ITO coated glass. The device has a low response time (about 1 s), a high redox stability (retained performance by 96.4% even after 1000 cycles), and a high coloration efficiency (1377 $cm^2\ C^{-1}$). The neutral and oxidized state photos of the ECD are presented in Figure 4.

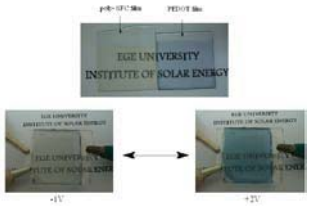

Figure 4. Neutral and oxidized state photos of SFC based electrochromic device

*Corresponding authors: 2Tserafettin.demic@ege.edu.tr,

[1] P.M.S. Monk, R.J. Morimer, D.R. Rosseinsky, Electrochromism: Fundamentals and Applications, VCH, Weinheim, Germany, 1995.
[2] K. S. Kim, Y. M. Jeon, J. W. Kim, C. W. Lee, M. S. Gong, Organic Electronics, 2008, 9, 797.
[3] Bloudin, N.; Leclerc, M. Acc. Chem. Res. 2008, 41, 1110-1119

In Vitro Bioavailability of Coenzyme Q10 in Meats and Enriched Yogurts with Emulsified CoQ10, γ-cyclodextrin CoQ10 Complex and Nanoparticle Coenzyme Q10 Preparations

Pinar Ercan[1], Sedef Nehir El[1]*
[1]*Food Engineering Department, Engineering Faculty, Ege University, 35100, Bornova, Izmir, Turkey*

Abstract-In this study, coenzyme Q10 bioavailabilities of samples (beef meat, beef liver, beef heart, yoghurt, yoghurt containing emulsified coenzyme Q10, yoghurt containing γ-cyclodextrin coenzyme Q10 complex and yoghurt containing nanoparticle coenzyme Q10) were compared. The highest coenzyme Q10 bioavailability was found in yoghurt containing nanoparticle coenzyme Q10.

Coenzyme Q10 (CoQ10) is a fat soluble, vitamin like benzoquinone compound and also an important antioxidant [1]. Coenzyme Q10 plays roles in membrane stability, energy transformation and ATP production [2, 3]. CoQ10 is supplied from two sources; endogenous synthesis and exogenous sources (foods and supplements) [4]. CoQ10 amounts in human decrease with age and some diseases. Therefore, information on exogenous sources of coenzyme Q10 is important. Bioavailability is the degree to which a substance becomes available to the target tissue after administration [5]. Coenzyme Q10 has a relatively high molecular weight (863 Da) and its solubility in lipids is also limited so it is very poorly absorbed in the gastrointestinal tract [5, 6]. Crane (2001) reported that to increase the concentration significantly requires in a day at least 100 mg coenzyme Q10 which can increase the level in blood to around 2 μg/mL or more. Even with large amounts of beef heart in the diet, it would be difficult to supply 100 mg/day [7]. The need for more information on the bioavailability of coenzyme Q10 is strongly stressed. This study were conducted in two parts, the aim of first part was to determine content CoQ10 in beef meat, beef liver, beef heart which are rich in CoQ10 and effect of some thermal processes on the bioavailabilities of CoQ10. In the second part, three CoQ10 preparations were produced with the reference CoQ10 standard. Emulsified coenzyme Q10, γ-cyclodextrin coenzyme Q10 complex and nanoparticle coenzyme Q10 were used enrichment of yoghurt samples. Also bioavailabilities of CoQ10 preparations were studied and compared.

Results from the present study indicated that meat samples especially beef liver and beef heart were found as important sources of coenzyme Q10. However, coenzyme Q10 contents of meat samples are not enough to supply 100 mg/day. Coenzyme Q10 contents were found as 109.97 ± 3.77 μg/g in beef heart, 33.34 ± 3.51 μg/g in beef liver and 23.47±2.59 μg/g in beef. The highest loss in coenzyme Q10 content was found as 30.58±1.37 % ($p<0.01$) in beef heart after frying processing. Coenzyme Q10 losses were also found as 23.62± 2.18 % and 22.81±2.66 % after frying of beef liver and boiling of beef meat, respectively. Bioavailabilities of coenzyme Q10 in beef heart (65.84±2.06 %) and beef liver (68.17±1.47 %) were higher than the bioavailability of coenzyme Q10 in beef (60.16±1.30 %) significantly ($p<0.01$).

One serving size of yoghurt (250 g) was enriched with 100 mg coenzyme Q10. In this study, in order to increase daily intake of coenzyme Q10 and the bioavailability emulsified coenzyme Q10, γ-cyclodextrin coenzyme Q10, nanoparticle coenzyme Q10 were prepared with the reference coenzyme Q10 standard which was purchased in the commercial form. The 15% coenzyme Q10 loaded poly DL-lactide-co-glycolide (PLGA) nanoparticles prepared by emulsion-diffusion-evaporation method was obtained as in spherical shape with 176.00±50.62 nm diameter. These coenzyme Q10 preparations were added into skim milk and used in the production of enriched yoghurts. The yoghurt containing nanoparticle coenzyme Q10 had the highest coenzyme Q10 bioavailability (73.81±1.61 %) among the samples ($p<0.01$). Coenzyme Q10 bioavailabilities were also found as 50.59±1.88 % in control yoghurt, 63.75±0.91 % in yoghurt samples containing emulsified CoQ10, and 46.83±1.27 % containing γ-cyclodextrin CoQ10 complex (Figure). A new product approach which had a high nutritional value was formed with the enriched yoghurts containing different coenzyme Q10 preparations. At the end of the comparison of bioavailabilities of enriched yoghurts with different coenzyme Q10 preparations, it was seen that the highest bioavailability reached with decreasing the particle size of coenzyme Q10 to nano size ($p<0.01$). These enriched yoghurts can increase the daily intake of coenzyme Q10 and it can be suitable for humans have some problems with endogenous synthesis.

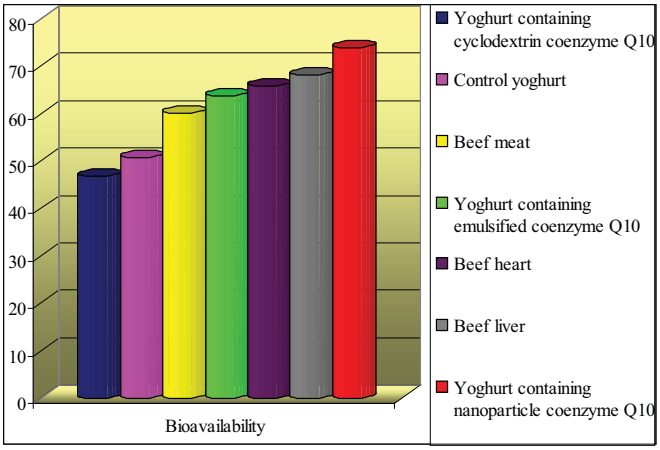

Figure 1. Coenzyme Q10 bioavailabilities of all samples.

The financial support of this study by The Scientific and Technological Research Council of Turkey - TÜBİTAK (Project no: 108O603) and 1TEge University Science and Technology Development and Research Center - EBILTEM (Project no: 09/BİL/013) are gratefully acknowledged.

*Corresponding author: sedef.el@ege.edu.tr

[1] Xia, S., Xu, S., Zhang, X., 2006, *J. of Agr. Food Chem.,* 54, 6358–6366.
[2] Kubo, H., Fujii, K., Kawabe, T., Matsumoto, S., Kishida, H., Hosoe, K., 2008. *J. Food Com. and Analysis*, 21: 199–210.
[3] Mattila, P.,Kumpulainen, J.,2001. *J. Food Com.and Anal.*,14:409-417.
[4] Overvad, K., Diamant, B., Holm, L., Hùlmer, G., Mortensen, S.A., Stender, S., 1999. *Euro. J. of Cl. Nutr.*, 53, 764±770.
[5] Žmitek, J., Žmitek, K., Pravst, I., 2008.*Agro*FOOD *industry hi-tech*,vol 19.
[6] Ankola, D.D., Viswanad, B., Bhardwaj, V., Ramarao, P., Kumar M.N.V.R., 2007. *Eur. J. of Phar. and Bioph.s*, 67, 361–369.
[7] Crane, F.L. (2001). Q10, *J. of the American College of Nutrition*, 20, 591–598.

Computational Insight into the Acceptor-Donor Type of Conducting Polymers Containing Pendant Fullerene Groups

Alimet Sema Özen[1*]
[1]*Faculty of Engineering and Natural Sciences, Sabancı University, İstanbul 34956, Turkey*

Abstract— In this study, it is proposed that solvent is an important parameter in the design of the low-band gap acceptor-donor type of conducting polymers containing integrated fullerene groups. The results of the extensive DFT and TDFT calculations are presented to support this proposal. This is the first computational study in the literature on that type of fullerene containing oligomers and on the solvent effect for conducting polymers in general.

Conducting polymers [1] have been extensively studied over the past three decades theoretically, synthetically and in terms of applications, ever since the discovery of the increase in the electrical conductivity of poly-acetylene when it was doped with iodine or other acceptors [2]. These polymers have large application areas in light-emitting diodes (LED), field-effective transistors (FET), solar cells, sensors, electro-chromic transistors, non-linear optics due to their high-conductivity and environmental stability properties. On the other hand, due to the processing problems encountered with doped conducting polymers, the ultimate goal has been the design of polymers featuring intrinsic conductivity properties. One successful approach has been the cooperation of electron donor and electron acceptor moieties in an alternating manner throughout the polymer backbone [1, 3-5]. It was found that band gap decreases drastically by the use of fullerene as the acceptor group and this was considered as an important step forward towards the design of zero band-gap polymers [6].

The aim of the present computational study is to determine the band-gap of the acceptor-donor type conducting polymer whose monomer is shown in Figure 1 and to examine the effect of the solvent on the band-gap of that type of structures where it is expected to observe a solvatochromic shift depending on the polarity of the solvent. Furthermore, the extent and effect of homoconjugation has also been investigated.

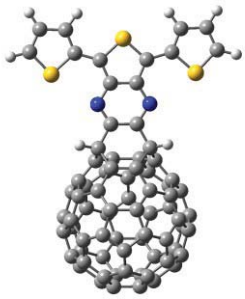

Figure 1: Monomer of the fullerene containing acceptor-donor type of conducting polymers

To accomplish this task, geometry optimizations were performed using density functional theory (DFT) as the computational method. The calculations were performed at the B3LYP/6-31G(d) and MPW1B95/6-31G(d) levels of theory. Excitation energies used in the calculation of the band gaps have been calculated by both the HOMO-LUMO difference of DFT optimized geometries and the vertical excitation energies by time-dependent DFT (TDDFT) [7] method at the same level. Semi-empirical ZINDO calculations were also performed on the DFT optimized geometries. Values calculated at the monomer, dimer and trimer levels are extrapolated to estimate the polymeric values [8]. Implicit solvent optimizations with o-dichloro benzene were performed using the polarized continuum model (PCM) of the self-consistent reaction field theory (SCRF) [9]. Explicit solvent optimizations were employed to understand the specific solute-solvent interactions and their effect on the band gap.

In the absence of the solvent (neither implicit nor explicit), the highest and lowest band gap values were obtained by MPW1B95 (1.71 eV) and TD-B3LYP calculations (1.01 eV), respectively. Since the lowest value is still a little bit higher than the experimental results, the solvent effect was thought to be more effective in determination of the band gap. Implicit solvent calculations using the PCM optimizations did not alter the HOMO-LUMO energy difference (for example, using the method MPW1B95, monomer HOMO-LUMO energy differences are 2.56 and 2.52 eV with and without solvent field, respectively). However, introduction of the explicit solvent molecules lowered the band gap (2.35 eV for the monomer with three solvent molecules at the MPW1B95 level). This value reduces to 1.80 eV when monomer vertical excitation energy is calculated by TDDFT/MPW1B95 method with explicit solvent molecules. This value is a good indicator or starting point for a small band-gap value after extrapolation with higher degree of oligomerization.

Homoconjugation was investigated using atoms-in-molecules (AIM) theory. No bond critical points were obtained as a proof of through-space conjugation. On the other hand, HOMO and LUMO molecular orbital diagrams show some electron delocalization between the fullerene ring and the thieno pyrazine group.

This work was supported by İTÜ-UYBHM Grant No. 10822009. Fruitful discussions with late Gürsel Sönmez and Canan Atılgan are gratefully acknowledged. This work is dedicated to the respectful memory of Gürsel Sönmez.

*Contact information: semaozen@sabanciuniv.edu

[1] Handbook of Conducting Polymers, 2nd ed.; Skotheim, T. A., Elsenbaumer, R. L., Reynolds, J. R., Eds.; Marcel Dekker: New York, 1998.
[2] (a) C. K. Chiang *et al*. *Phys. Rev.Lett.* **39**, 1098 (1977). (b) N. Basescu *et al. Nature* **327**, 405 (1987).
[3] A. Ajayaghosh,. *Chem. Soc. Rev*. **32**, 181 (2003).
[4] H. A.M. Van Mullekom *et al. Mater. Sci. Eng.* **32,** 1 (2001).
[5] H. A. M. Van Mullekom, J.A.J. M.Vekemans, E.W. Meijer, *Chem.Eur. J.* **4**, 1235 (1998)
[6] G. Sonmez *et al. Adv. Mater*. **17**, 897 (2005).
[7] E.K.U: Gross, W. Kohn, *Adv. Quantum Chem.* **21**, 255 (1990).
[8] S. Yang,P. Olishevski, M. Kertesz *Synth. Met.* **141**, 171 (2004).
[9] J. Tomasi, B. Mennucci, R. Cammi, *Chem. Rev*.**105**, 2999 (2005).

Carrier transport and efficiency retention in InGaN light emitting diodes at high injection levels

Ü. Özgür,[1,*] X. Ni,[1] X. Li,[1] J. Lee,[1] S. Liu,[1] V. Avrutin,[1] A. Matulionis,[2] and H. Morkoç[1]

[1]*Department of Electrical and Computer Engineering, Virginia Commonwealth University, Richmond, VA 23284, USA*
[2]*Fluctuation Research Laboratory, Semiconductor Physics Institute, Vilnius, Lithuania*

Abstract—InGaN light emitting diodes (LEDs) are destined to become a key component of the lighting technology as light sources of blue, violet, and green as well as white light emitters when used in conjunction with fluorescent dyes. However, the external quantum efficiency of InGaN LEDs reaches a maximum at current densities as low as 50 A/cm^2, followed by a monotonic decrease with increased injection, which, unless rectified, would be detrimental for their insertion into the general lighting market. The commonly proposed physical origins for this loss of efficiency are Auger recombination, electron overflow (spillover), current crowding, asymmetric injection of electrons and holes, and poor transport of holes through the active region. While the Auger recombination received the early limelight, increasing body of data seem to be inconsistent with this mechanism but appear to support the electron overflow model. We have investigated LEDs with different active region structures and polar *c*-plane and nonpolar *m*-plane orientations, to shed the much needed light on the carrier injection and transport in InGaN LEDs. The experimental results together with carrier transport simulations strongly suggest that electron overflow, which can be mitigated with careful design of the LED active region and by using m-plane orientation that supports higher hole concentrations and larger optical matrix elements compared to c-plane, is responsible for the loss of efficiency in InGaN LEDs at high injection levels. In this presentation, details of both the electroluminescence and all optical measurements forming the basis for the data sets and the transport model developed will be discussed.

*Corresponding author: uozgur@vcu.edu